ISPRS Journal of Photogrammetry and Remote Sensing 128 (2017) 40–46

Contents lists available at ScienceDirect

ISPRS Journal of Photogrammetry and Remote Sensing

journal homepage: www.elsevier.com/locate/isprsjprs

Characterisation and improvement of the structure function estimation for application in PSI

Franz-Georg Ulmer *, Nico Adam

Deutsches Zentrum für Luft- und Raumfahrt (DLR), Institut für Methodik der Fernerkundung, Münchener Straße 20, 82234 Weßling, Germany

ARTICLE INFO

Article history:
Received 22 June 2016
Received in revised form 23 December 2016
Accepted 13 March 2017

Keywords:
Weather Research and Forecasting model (WRF)
Numerical Weather Prediction (NWP)
DInSAR
Zenith Time Delay (ZTD)
Global Positioning System (GPS)
Refraction

ABSTRACT

Numerical Weather Prediction (NWP) is becoming state of the art for the compensation of atmospheric effects in InSAR and especially in PSI. The structure function (variogram) estimated on the InSAR data and on the NWP data is a required statistical characteristic and very useful in the processing of the data. For example, the structure function (typically the semivariogram) estimated on InSAR data is fundamental for the Kriging of the atmospheric phase screen (APS) based on irregular PSI estimates. The required parameters are the nugget, the range and the slope of the structure function. The practical implementation has shown that the NWP predicted structure function and the InSAR estimated structure function based on the conventional semivariogram equation do not match. Straightforward explanations are wrongly estimated APSs due to an insufficient number of interferograms or hindcasts that fail to capture the turbulent water vapour signal. However, in this paper we explain the effects of noise in interferograms and coarse resolution in the NWP on the conventional structure function estimation resulting in the observed mismatch. In order to avoid the mismatch, an alternative implementation based on wavelets is suggested and demonstrated using real Sentinel-1 data. We show that the wavelet based structure function estimation outperforms the conventional structure function estimation based on a variogram. Application of the proposed structure function alternative based on NWP data are the master selection, the estimation of the effective NWP data resolution, and a statistical consistency check of the estimated InSAR APS. To support the understanding, we demonstrate the effects of noise and resolution using simulated fractals. An application of the proposed wavelet based structure function estimation is the estimation of the effective NWP data resolution, which is demonstrated using the same Sentinel-1 data test case.

1. Introduction

SAR interferometry has become a powerful remote sensing tool for the monitoring of subtle deformations on the Earth's surface. During the SAR acquisition, the atmosphere maps into the interferometric phase as the atmospheric phase screen (APS) because it affects the propagation velocity of the radar wave. It is a well-known fact that the APS is the dominant error source for InSAR (Hanssen, 2001). In PSI (see Ferretti et al., 2001), the APSs of n interferograms (Φ_i) are mitigated by two processing steps. First, the APSs (X_i) are hindcast by a numerical weather model and are subtracted from the interferograms ($\hat{\Phi}_i = \Phi_i - X_i$), mitigating the low-frequency component in space and the vertical stratification effect. Unfortunately, a water vapour related high-frequency APS component is still present ($\hat{\Phi}_i$) because of the chaotic behaviour of convection that transports the water vapour. Second, a time series analysis of the interferograms ($\hat{\Phi}_1, \ldots, \hat{\Phi}_n$) on a reference network of temporal coherent persistent scatterers (PSs) allows estimation of the residual APS signal. The dependence of APS variance on the spatial distance between two points of interest can be described using structure functions. This characterisation allows spatial interpolating and filtering of the irregularly sampled APS signal by Kriging. The required semivariogram is estimated from the hindcast APS or from the interferometric data directly with the nugget, the range and the slope of the structure function. The APS compensation supported by NWP is a recent development. Hindcast water vapour, pressure and temperature can be transformed into refractivity and finally into an APS prediction (X_i) (Holley et al., 2007; Jung et al., 2014; Nico et al., 2011; Adam, 2013; Pierdicca et al., 2011; Perissin et al., 2011; Smith and Weintraub, 1953; Ulmer and Adam, 2015). Surprisingly, the

* Corresponding author.
E-mail addresses: Franz-Georg.Ulmer@dlr.de (F.-G. Ulmer), Nico.Adam@dlr.de (N. Adam).

http://dx.doi.org/10.1016/j.isprsjprs.2017.03.005
0924-2716/

conventional variogram estimation applied on InSAR and NWP data independently results in structure functions that do not match. This is unexpected because both describe the same atmospheric effect. This effect is also reported by Gong et al. (2010). We show in this paper that this observed mismatch can be explained by biases in the conventional structure function estimation process that are caused by noise in the original interferograms as well as by the low resolution of available NWPs. In order to avoid the discrepancy, an alternative implementation based on wavelets is suggested and demonstrated using real Sentinel-1 data. In doing so, we show that the wavelet based structure function estimation is more suitable for PSI compared to the conventional structure function estimation based on a variogram. As a consequence, the proposed structure function alternative assists the master selection, the estimation of the effective resolution of the NWP data and a statistical consistency check of the estimated InSAR APS. To support the understanding, we demonstrate the effect of noise and resolution using simulated fractals.

The objective of the paper is to better support the estimation of the APS in PSI by providing an improved statistical characterisation of the APS. The proposed estimation of the structure function allows consistent structure function estimates based on InSAR and NWP data. Another objective is the explanation of the two effects biasing the conventional estimation.

2. Methods

The dependence of APS variance on the spatial distance between two points of interest can be described using structure functions. Commonly, closely located points are stronger correlated compared to points with larger distances. Therefore, the variability of the changes between two points is larger the more they are further apart. In the case of APS, this distance-variability relationship follows a power law and can be modelled by the fractional Brownian motion process (Hanssen, 2001). The distance-variability relationship is derived by considering two arbitrary points (p_1, p_2) of the APS (X_{p_1}, X_{p_2}) with distance $s = |p_1 - p_2|$ and the APS change $X_s = X_{p_2} - X_{p_1}$. The following self-similarity property of fractional Brownian motion processes describes the variance relationship between different scales and is essential to derive the following equations. This property states that the variance $\mathrm{V}(X_s)$ is equal to

$$\mathrm{V}(X_s) = \mathrm{V}(s^H X_1) \quad (1)$$
$$= s^{2H}\mathrm{V}(X_1) \quad (2)$$

where H is the Hurst exponent and $\mathrm{V}(X_1)$ is the variance of the APS at the distance of one [km] for simplicity. Correspondingly, the following equations are derived.

$$\log(\mathrm{V}(X_{p_2} - X_{p_1})) = \log(\mathrm{V}(X_s)) \quad (3)$$
$$= \log(\mathrm{V}(s^H X_1)) \quad (4)$$
$$= \log(s^{2H}\mathrm{V}(X_1)) \quad (5)$$

As a result, we can decompose the right hand side into

$$= \log(s^{2H}\sigma_X^2) \quad (6)$$
$$= \log(\sigma_X^2) + 2H\log(s) \quad (7)$$

where $\sigma_X^2 = V(X_1)$. Therefore, the linear log(variance)-log(range) slope is related to the Hurst exponent H by the factor of two.

2.1. Effect of noise on the structure function estimation

A statistic model is developed in this section that is used to explain the biasing effect of noise on structure function estimates. In PSI, the APS estimates are affected by noise due to the limited phase precision. The noise is unavoidable and can be parameterised by the signal to clutter ratio (SCR) describing the quality of a persistent scatterer (PS). The PSs with their respective quality are given by chance and, therefore, additive noise needs to be considered in the practical structure function estimation. To develop the statistical model, the characterisation of the noise distribution is of interest whereas its actual density function is not. To be more specific, it is not assumed that the noise is Gaussian distributed but it is assumed that the noise distribution has a second moment. Noise Y_i with expectation $\mathrm{E}(Y_i) = 0$ and variance $\mathrm{V}(Y_i) = \sigma^2$ is added to the APS X, denoted by $X'_{p_1} = X_{p_1} + Y_1$ and $X'_{p_2} = X_{p_2} + Y_2$ to derive the framework. In doing so,

$$\log(\mathrm{V}(X'_{p_2} - X'_{p_1})) = \log(\mathrm{V}(X_s + Y_2 - Y_1)) \quad (8)$$
$$= \log(\mathrm{V}(X_s) + 2\sigma^2) \quad (9)$$
$$= \log(\mathrm{V}(s^H X_1) + 2\sigma^2) \quad (10)$$
$$= \log(s^{2H}\sigma_X^2 + 2\sigma^2). \quad (11)$$

Accordingly, the log(variance)-log(range) plot is no longer linearly related. This can be seen in Fig. 4(a) and is discussed in detail in the results section. The term $2\sigma^2$ dominates the term $s^{2H}\sigma_X^2$ for short length scales $s < \left(\frac{\sqrt{2}\sigma}{\sigma_X}\right)^{\frac{1}{H}}$, such that the corresponding plot is nearly constant for small ranges.

2.2. Effect of coarse resolution on the structure function

In NWP, the atmosphere state is simulated by solving a set of partial differential equations. These are solved for fixed volume elements. Typically, the volume elements have a spatial resolution in the order of 3 km which can be further improved to 900 m by spending more computational resources. However, the size of the volume element always affects the estimation of the structure function because of the averaging representation of the respective atmospheric state in that volume. The averaging representation is the reason for the decreased variability visible in the structure function. This paper focuses on this effect. However, there is of course another uncertainty related to the temporal domain which is not considered here. A solution for this uncertainty is proposed in Ulmer and Adam (2015).

Next, the influence of the NWP resolution on the corresponding structure function is modelled. Therefore, a short length scale ($s_S > 0$) and a long range scale ($s_L > 0$) are considered for simplicity in [km]. The short length scale equals the effective resolution, which can be resolved by the NWP model. It is known that the APS is modelled by a fractal (see Hanssen, 2001) and is therefore described by a stationary fractional Brownian motion process, which is characterised by the Hurst exponent H. First, the APS X_t at position t is modelled as fractional Brownian motion process and its change (δX) at two different positions (p_1, p_2) is defined by

$$\delta X = X_{p_2} - X_{p_1}. \quad (12)$$

Second, it is assumed, that a point $p_M = p_1 + s_S$ is located between the two points and, therefore:

$$|p_2 - p_1| = s_S + s_L. \quad (13)$$

For simplicity, $E(X_1^2) = 1$ is assumed, which describes the APS change variability at one [km] range. The definitions above are illustrated in Fig. 1. Taking into account that $X_{p_M} = X_{p_1} + X_{s_S}$ and $X_{p_2} - X_{p_1} = X_{s_S} + X_{s_L}$ it follows

$$X_{s_S} = X_{p_M} - X_{p_1} \text{ and} \quad (14)$$
$$X_{s_L} = X_{p_2} - X_{p_M}. \quad (15)$$

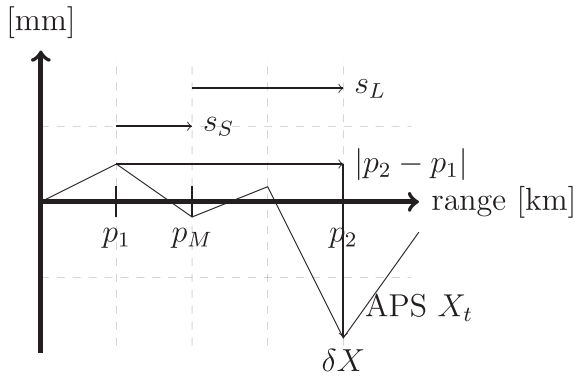

Fig. 1. Illustration of the definitions.

In doing so,

$$\mathrm{V}(\delta X) = \mathrm{V}(X_{p_2} - X_{p_1}) \tag{16}$$

$$= \mathrm{V}(X_{p_2} - X_{p_M} + X_{p_M} - X_{p_1}). \tag{17}$$

And because only the distance matters (stationarity), it follows that:

$$= \mathrm{V}(X_{s_L} + X_{s_S}) \tag{18}$$

$$= \mathrm{V}(X_{s_L}) + \mathrm{V}(X_{s_S}) + \underbrace{\left(|s_S|^{2H} + |s_L|^{2H} - |s_S - s_L|^{2H}\right)}_{2\mathrm{Cov}(X_{s_S}, X_{s_L})}. \tag{19}$$

The step from Eq. (18) to Eq. (19) is valid because of the definition of the fractional Brownian motion process which is given by

$$2\mathrm{Cov}(X_{s_S}, X_{s_L}) = (|s_S|^{2H} + |s_L|^{2H} - |s_S - s_L|^{2H}). \tag{20}$$

For the NWP, $\mathrm{V}(X_{s_S}) = 0$ whereas $\mathrm{V}(X_{s_S}) \neq 0$ for the interferogram because s_S is not resolved by the NWP but resolved by the interferogram. This causes an offset in the structure function estimation between both, as illustrated in Fig. 2. Since, s_S is not resolved by the NWP no signal is present ($X_{s_S} = 0$). Accordingly, $\mathrm{Cov}(X_{s_S}, X_{s_L}) = 0$ for the NWP for each H but $2\mathrm{Cov}(X_{s_S}, X_{s_L}) = \left(|s_S|^{2H} + |s_L|^{2H} - |s_S - s_L|^{2H}\right) \neq 0$ for the interferogram in case of $H \neq \frac{1}{2}$. Depending on H

$$\mathrm{Cov}(X_{s_S}, X_{s_L}) \text{ is } \begin{cases} > 0 & \text{if } H > \frac{1}{2} \\ = 0 & \text{if } H = \frac{1}{2} \\ < 0 & \text{if } H < \frac{1}{2} \end{cases}. \tag{21}$$

Practically, $2\mathrm{Cov}(X_{s_S}, X_{s_L})$ is increasing for the APS of the interferogram if s_L increases, because $H \approx 0.7$ for $s_L > 2$ [km] (see Hanssen, 2001). Correspondingly, the slope of the red[1] structure function plot is underestimated by the NWP compared to the interferogram. This is illustrated in Fig. 2.

2.3. Wavelet based structure function estimation

Based on the work from Nelson and Kingsbury (2010), a more suitable analysis is now explained. Utilized is the dual tree complex wavelet transform ($DT\mathbb{CWT}$) which is broadly used in computer vision. Basically, it is a wavelet transform with directional wavelets and has some advantages such as shift invariance in contrast to the straightforward discrete wavelet transform (see Selesnick et al., 2005). Different wavelet domains represent different spatial frequencies and act like a filter in our approach. NWPs have a much coarser resolution (s_S) compared to an interferogram.

[1] For interpretation of colour in Fig. 2, the reader is referred to the web version of this article.

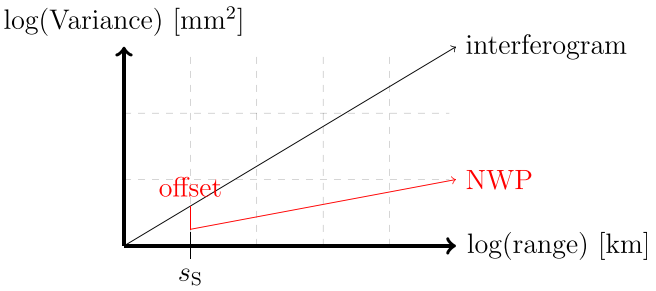

Fig. 2. Illustration of the structure function estimates.

Correspondingly, higher frequencies than $\frac{1}{s_S}$ are not considered. The $DT\mathbb{CWT}$ analysis provides six directional sub-bands for each frequency domain. Correspondingly, o frequency domains consist of $m = 6o$ sub-bands. For the structure function estimation, the sample variances for the m sub-bands $(W_1, \ldots, W_m)$

$$\hat{\mathrm{V}}(W_i) = \frac{1}{2n} \sum_{c \in W_i} \mathrm{r}(c)^2 + \mathrm{i}(c)^2 \tag{22}$$

are computed where n coefficients c are within W_i and $r(c)$ and $i(c)$ are the real and imaginary parts of c, respectively. The APS is a fractional Brownian motion process and is therefore characterised by the self-similar property, i.e. $\mathrm{V}(X_{2s}) = 2^{2H}\mathrm{V}(X_s)$. Correspondingly, the sample variances of different scales are related by the power law.

2.4. APS computation from NWPs

In the results section, we compare a predicted NWP APS with an observed DInSAR APS. The hindcast APS processing is now described in detail. First, two weather research and forecasting (WRF) model hindcasts for different dates (t_1, t_2) related to the two SAR satellite acquisitions are computed. Second, the APS $(\hat{X}_t)$ related to the t-th SAR acquisition is computed. Each APS is composed of a hydrostatic term corresponding to (refractivity N_h) and a wet term corresponding to (refractivity N_w). Both are influenced by temperature (T). The hydrostatic term is additionally related to the total pressure (P) while the wet term depends on the water vapour (e). Based on physics, the range distance deviation is defined by

$$\hat{X}_t = 10^{-6} \int_{\vec{\boldsymbol{p}}_{(i,j)}}^{\vec{\boldsymbol{s}}} N(\vec{\boldsymbol{v}}) \mathrm{d}\vec{\boldsymbol{v}} \tag{23}$$

where

$$N = \underbrace{K_1 \frac{P}{T}}_{N_h} + \underbrace{K_2 \frac{e}{T} + K_3 \frac{e}{T^2}}_{N_w}. \tag{24}$$

$\vec{\boldsymbol{p}}_{(i,j)}$ is the three-dimensional location on Earth of the actual DInSAR pixel and $\vec{\boldsymbol{s}}$ is the position of the SAR satellite. Eq. (24) models the refractivity (N) and the coefficients (K_1, K_2, K_3) are provided by Rüeger (2002). Practically, for every pixel of the SAR-image, integration through the predicted three-dimensional atmospheric state produces an APS $(\hat{X}_t)$ related to time t. Finally, the DInSAR APS X is computed by $X = \hat{X}_{t_1} - \hat{X}_{t_2}$ while t_1 is the date of the master acquisition and t_2 is the date of the slave scene.

3. Results

First, the practical estimation problems of structure functions are demonstrated by two synthetic data experiments. Second, the

proposed wavelet based estimation analysis is tested on the Mexico City test case using Sentinel-1 data.

3.1. Experiment using synthetic data sets

In order to demonstrate the estimation effects, a noise free fractal (representing the ideal APS) is generated and additionally down-sampled depicting the hindcast coarse resolution APS from NWP (see Fig. 3(a) and (c)). For the noise free fractal and the simulated NWP APS, the structure function plot is presented in Fig. 4 (b). Second, the noise free fractal is deteriorate by additional noise (see Fig. 3(b)) and the structure functions of disturbed and undisturbed fractals are displayed in Fig. 4(a).

3.1.1. The noise issue

First, the flattening effect caused by white noise is demonstrated and a SNR of 7.28 and a Hurst exponent $H = 0.7$ are simulated. Therefore, the fractal is deteriorated by white noise (see Fig. 3(b) for $H = 0.7$) and the corresponding conventional structure functions of the noisy and the noise free fractal are compared. For short range scales, the noise term $2\sigma^2$ in Eq. (11) dominates the linear dependency term $s^{2H}\sigma_X^2$ and results in a flattened structure function. This is illustrated in Fig. 4(a) and confirms the noise effect. In contrast, the wavelet based alternative is much less affected by noise. A scatterplot is shown to illustrate this robustness. The biasing effect would result in a bent scatterplot while a perfect affine relationship $y = x$ and ideal correlation coefficient $R = 1$ reports the equality of the compared estimates. Here, the equality $y = x$ is interpreted as perfect affine relationship. The robustness is shown in Fig. 5(a) which compares the variance estimations of the fractal and the noisy fractal. The affine relationship $y = 0.94x + 0.59$ of this scatterplot demonstrates that there is no bias which significantly disturbs the perfect affine relationship $y = x$. Further, the very good correlation $R = 0.998$ between the variance estimations of nearly one illustrates the variance estimation independence in the presence of noise. To be exact, the first two wavelet domains are dominated by noise and are for this reason not considered. However, this separation of signal and noise demonstrates the advantage of the wavelet based alternative compared to the conventional structure function.

3.1.2. The coarse resolution issue

Commonly, APS with distances larger 2 km are characterised by the Hurst parameter $H \approx 0.7$ (see Hanssen, 2001). In this demonstration, three fractals of size 1024×1024 samples with Hurst parameters 0.3, 0.5 and 0.7 are generated using the power-law spectral technique (see Fig. 3(a) for $H = 0.7$). They represent the noise free APS of interferograms. The corresponding hindcast APS from the NWP has a 8×8 samples dimension, assuming a resolution of 10 m for the SAR acquisition and a resolution of 1280 m for

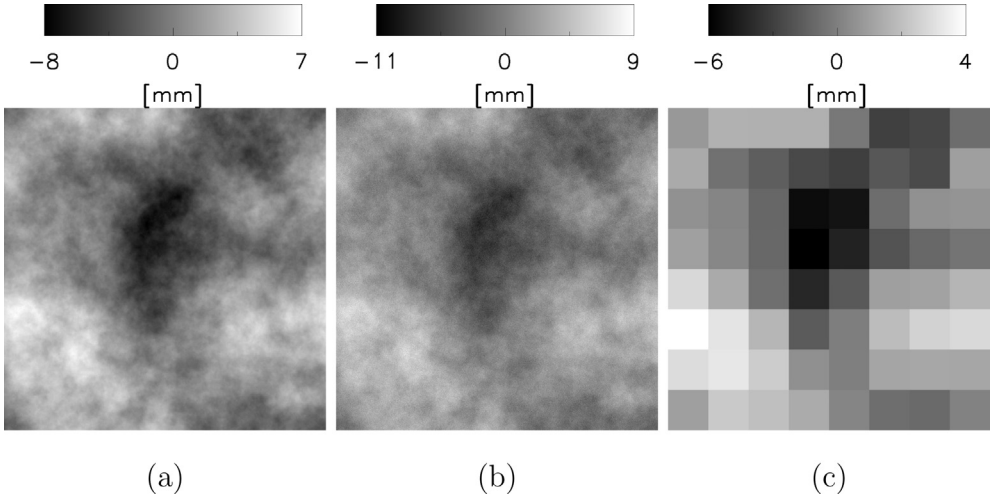

Fig. 3. Synthetic data with $H = 0.7$ (a) noise free APS (b) noisy APS (c) down-sampled noise free APS i.e. simulated NWP.

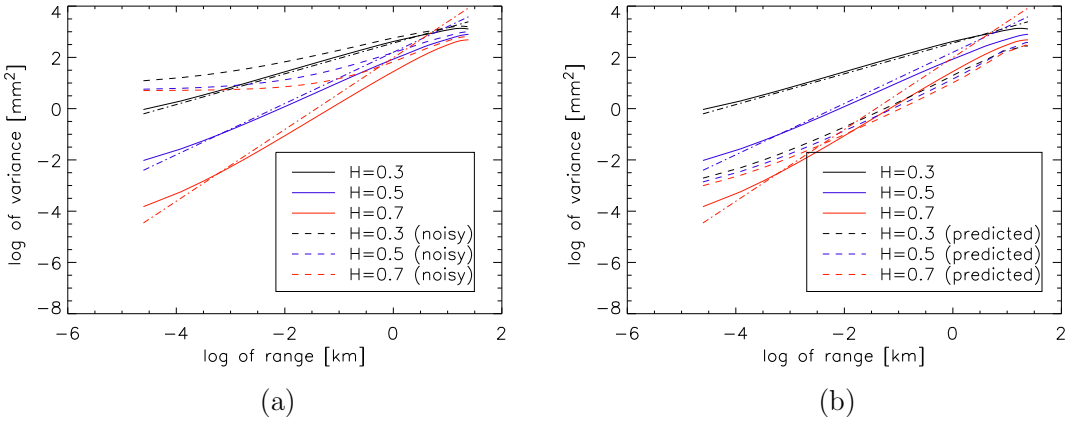

Fig. 4. Solid lines are the structure functions estimated from noise free fractals. Dashed lines illustrate the effect on the structure function estimation caused by (a) additional noise and (b) lower resolution hindcasts. Since APS are characterised by the Hurst parameter $H \approx 0.7$ (see Hanssen, 2001), the corresponding lines are bold and red. Theoretical straight lines (– · –) representing a Hurst exponent are plotted in the corresponding colour.

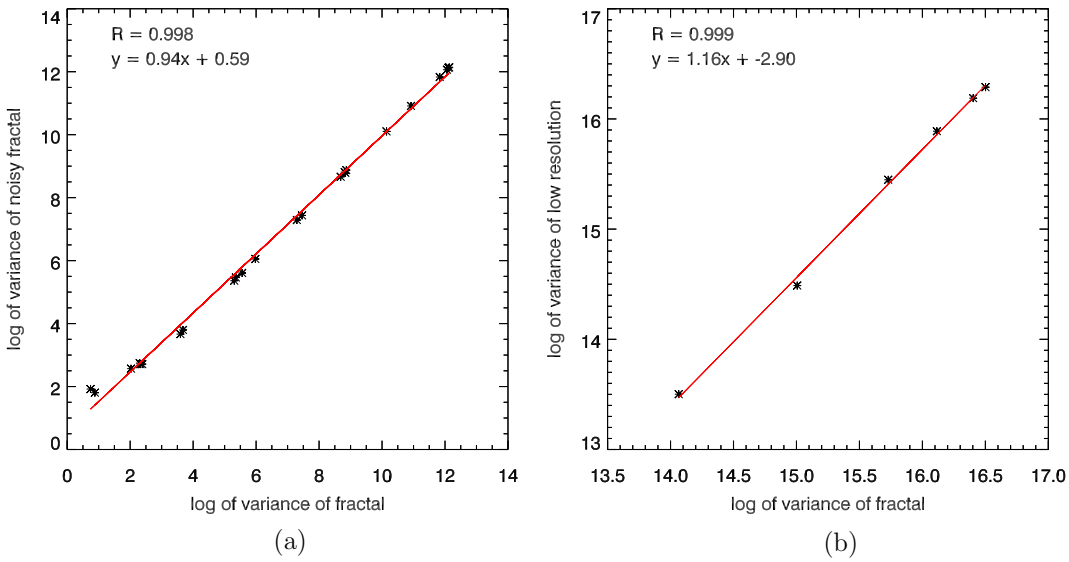

Fig. 5. Scatter plots of the wavelet domain variances between the fractal, (a) the noisy fractal and (b) the coarse prediction. A biasing effect would result in a bent curve while perfect matching estimates would result in an affine relationship $y = x$ and correlation coefficient $R = 1$.

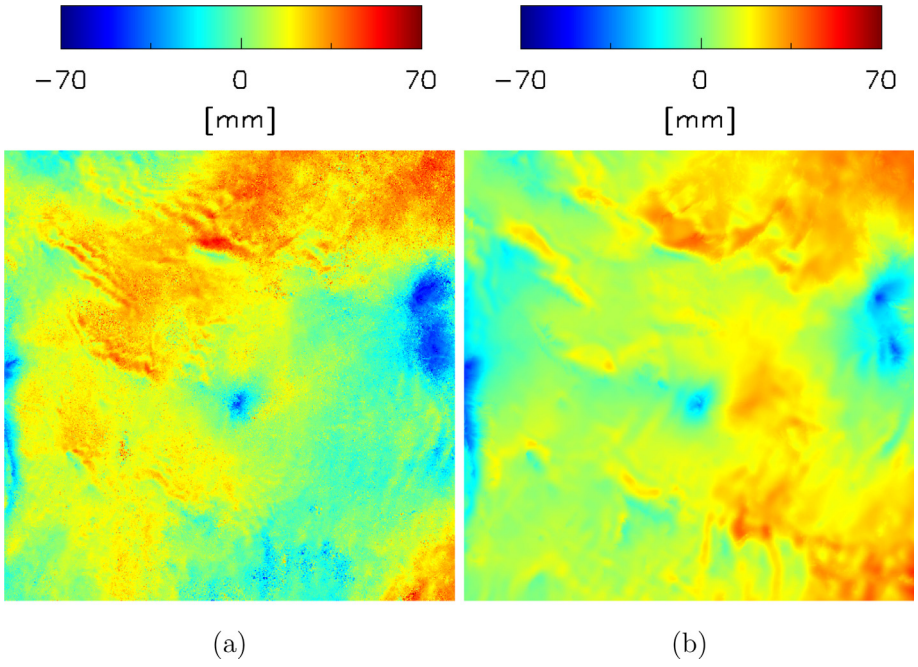

Fig. 6. (a) The interferogram of the acquisitions 2014-12-02 and 2014-11-08 and (b) the corresponding predicted APS derived by two WRF hindcasts of the corresponding dates.

the NWP (see Fig. 3(c) for $H = 0.7$). This is achieved by averaging 128×128 pixels of the fractal. The structure functions from the simulated APS and the hindcast APS are displayed in Fig. 4(b). The term $V(X_{s_S})$ of Eq. (19) causes an offset of the structure function which is nicely visible for $H = 0.5$. Additionally, the term $2\mathrm{Cov}(X_{s_S}, X_{s_L})$ from Eq. (19) causes an overestimation (black) of the slope for $H = 0.3$, an underestimation (red) of the slope for $H = 0.7$ and confirms therefore the statistical framework.

Next, it is illustrated that the wavelet based alternative can suppress spatial frequencies which are not resolved by a NWP. Therefore, the variance estimations of the fractal and the coarse prediction are compared. The first 7 wavelet domains are skipped and the lower resolution wavelet domains compared. The resulting scatter plot is shown in Fig. 5(b). Again, the affine relationship $y = 1.16x - 2.9$ is close to the perfect affine relationship $y = x$ and the correlation coefficient $R = 0.999$ is very close to the ideal correlation $R = 1$. Both characteristics testify that there is no biasing effect. For this comparison, a larger fractal of dimension 4096×4096 have to be considered, because otherwise too less wavelet domains would be present. However, the ability to suppress unresolved frequencies demonstrates the advantage of the wavelet based alternative analysis compared to the conventional structure function.

3.2. Demonstration of wavelet based estimation using Sentinel-1 data

For the experimental validation of the predicted APS from the WRF model, four short term interferograms $(\Phi_1, \Phi_2, \Phi_3, \Phi_4)$ of Mexico City generated from Sentinel-1 data are compared with respect to the predicted APS (an example is presented at Fig. 6). Therefore, the predicted APSs are computed from hindcasts which are described in detail in Section 2.4. In this demonstration, a clipped

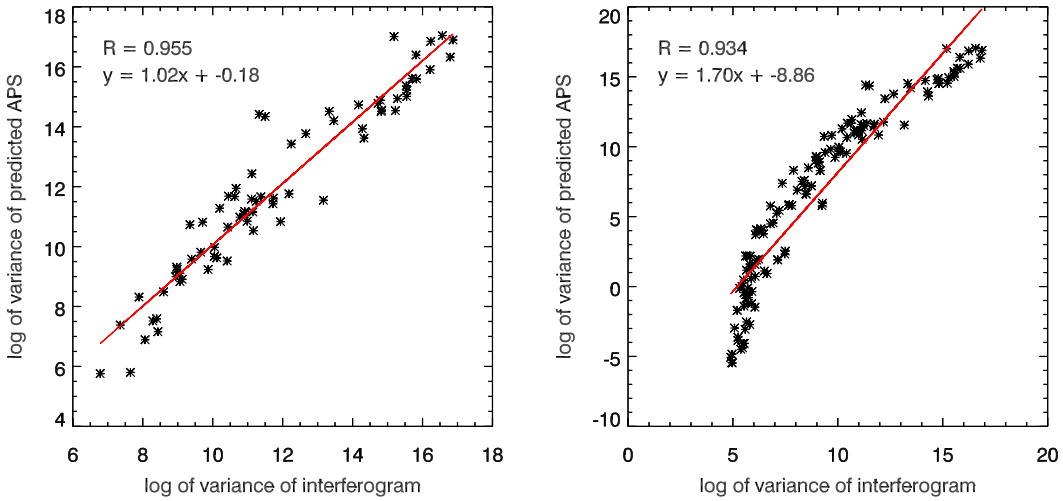

Fig. 7. Scatterplot of the sample variances from different wavelet domains between the observed interferograms APSs ($\Phi_1, \Phi_2, \Phi_3, \Phi_4$) and the hindcast APSs. (a) First three wavelet domains are skipped; (b) all wavelet domains are considered.

area of the full Sentinel-1 scene is considered, because the wavelet analysis needs a $2^m \times 2^m$ interferogram size where m is an arbitrary natural number. In this particular case, it corresponds to a spatial area of about 149 km × 143 km and is located eastwards of Mexico City. The date of the master scene is 2014-12-02 whereas the dates of the slave scenes are 2014-10-27, 2014-11-08, 2014-12-14 and 2014-12-26. For the hindcast APS, the NWP has been set up to a 900 m horizontal resolution. The utilized wavelet provided by Selesnick (2002) is of length 12 with three vanishing moments and with specified degree of three. It best estimated the Hurst exponent H of the synthetic data in previous tests. The first three wavelet scales were skipped, which match a resolution of 429 m in our case. Sample variances of the remaining wavelet domains of the predicted APSs and the interferograms ($\Phi_1, \Phi_2, \Phi_3, \Phi_4$) are compared with respect to each other. The corresponding scatter plot based on different scales and orientations is shown in Fig. 7 (a). The slope of the linear relationship is close to one and therefore unbiased, reflecting physical correctness of the NWP hindcast and demonstrates the advantage of this technique compared to the straightforward variogram analysis. Furthermore, the effective resolution s_S for the APS mitigation is measured, by skipping the first wavelet domain scales until the linear relationship is close to one. The relationship between a wavelet domain and its resolution is now described. A wavelet domain represents a wavelet with a spatial coverage and that coverage is doubled at each stage. The spatial resolution R_i of the wavelet domain i is derived by

$$R_i = 2^i w_0 R \tag{25}$$

where w_0 is the count of non-zero numbers of the starting one-dimensional wavelet and R is the resolution of the DInSAR. Correspondingly, the sharp curvature in Fig. 7(b) defines the effective resolution; in our case, 858 m.

The proposed structure function estimation has two valuable applications in PSI. First, it enables a statistical consistency check of the estimated InSAR APS. For this, the $\log(\hat{V}(W_i))$ of the predictions and the interferogram are compared. Second, the effective resolution of the NWP hindcast is confirmed.

4. Discussion

The wavelet based estimation of the structure function allows estimating the physically correct fractal dimension independent of additive noise and input data resolution. As a result, it provides compatible estimates based on InSAR and NWP input data. For example, in practice, the proposed technique resolves the limitations of the conventional variogram estimation. The conventional variogram estimation requires noise free InSAR data and an averaging of the APS to the NWP resolution in order to provide matching structure functions between InSAR and NWP.

A by-product of the wavelet based estimation is the effective resolution of the input data. The algorithm applied on the NWP data verifies the quality of the used weather model software, initialisation data and parameter setting. Applied on the Kriged PSI APS data, the effective resolution is of value because the APS is estimated from an irregular grid of PSs which are given by chance. Depending on the PS density and quality, the resolution is a characteristic of the actual test site.

An application of the wavelet based estimator is the master scene selection for PSI. Based on an APS prediction from NWP data, the domain variances of the first resolution domains can be used to compare the impact of the actual atmosphere effect. The best choice is the APS with the largest wavelet domain for which the variance is below a threshold. The threshold corresponds to the variance allowing to correctly estimate the topography update and velocity between two persistent scatterers. The difficulty in comparing interferograms and NWP APSs is caused partly by noise in the interferograms but mainly by the NWP data due to the much coarser resolution. Of course, the resolution of the NWP can be improved, however, the computational effort becomes too large. For example, if the desired resolution is 300 m instead of 900 m, the temporal integration step size has to be a third of the 900 m resolution computation. Furthermore, the grid size increases by at least a factor of 9. Therefore, the computation for the 300 m resolution takes about 27 times longer than for the 900 m resolution. Unfortunately, the benefit for APS mitigation is not clear, because WRF uses a digital elevation model (DEM) with a resolution of a maximum 30 arc seconds which is about 900 m. This DEM can be exchanged by one with a better resolution but then the hindcast becomes more unstable.

A practical implementation of the proposed technique could be as follows. The NWP resolution is chosen depending on the computational resources and the threshold for unbiased wavelet domains of the NWP APSs is given by Eq. (25). An example is our test case where the effective resolution of 858 m is approximately 900 m, which equals the NWP resolution. The effective resolution may vary for other weather models, parametrisations or input weather data. The proposed technique is demonstrated using Sentinel-1

data but is also applicable to high-resolution SAR data. It is best used for the pure turbulent APS component. This can be achieved by a compensation of the vertical stratification component using a coarse NWP and a high-resolution DEM. This is not a practical restriction since it is a systematic effect with little sensitivity to errors in the NWP prediction.

5. Conclusion

A robust structure function estimation has been proposed. It is suitable to provide consistent estimates obtained from InSAR and NWP independently. As a consequence, it supports the estimation of the Kriging parameter for PSI based on NWP data which advantageously are noise free and given on a regular sampling raster. It also supports the master scene selection, the estimation of the effective resolution of the NWP data and a statistical consistency check of the estimated InSAR APS. The effects influencing the estimations, namely the additive noise and the low resolution (corresponding to averaging of high resolution domains) are described and practically demonstrated with a simulated fractal. The application of the algorithm on real Sentinal-1 data also demonstrates the robustness with respect to the additive noise and the averaging effect and finally the practical applicability.

Acknowledgement

We thank our colleagues Fernando Rodriguez who provided the Mexico City InSAR data, Xiaoying Cong and Allessandro Parizzi for the comments that greatly improved the manuscript.

References

Adam, N., 2013. Algorithmic PSI Improvement in Mountainous Areas by Atmosphere Mitigation. Technical Report. DLR. <http://elib.dlr.de/95190/1/AtmosphereMitigation_v3.10.pdf>.

Ferretti, A., Prati, C., Rocca, F., 2001. Permanent scatterers in SAR interferometry. IEEE Trans. Geosci. Remote Sens. 39, 8–20.

Gong, W., Meyer, F., Webley, P.W., Morton, D., Liu, S., 2010. Performance analysis of atmospheric correction in InSAR data based on the weather research and forecasting model (WRF). In: Geoscience and Remote Sensing Symposium (IGARSS), 2010 IEEE International. IEEE, pp. 2900–2903.

Hanssen, R., 2001. Radar Interferometry: Data Interpretation and Error Analysis. Remote Sensing and Digital Image Processing. Springer <http://books.google.de/books?id=bqNkJUk4wtMC>.

Holley, R., Wadge, G., Zhu, M. (Eds.), 2007. New insights into the nature and effects of the water vapour field on InSAR measurements over Etna, FRINGE <http://earth.esa.int/fringe07/participants/159/pres_159_holley.pdf>.

Jung, J., Kim, D., Park, S.E., 2014. Correction of atmospheric phase screen in time series InSAR using WRF model for monitoring volcanic activities. IEEE Trans. Geosci. Remote Sens. 52, 2678–2689. http://dx.doi.org/10.1109/TGRS.2013.2264532.

Nelson, J.D.B., Kingsbury, N.G., 2010. Dual-tree wavelets for estimation of locally varying and anisotropic fractal dimension. In: ICIP. IEEE, pp. 341–344 <http://dblp.uni-trier.de/db/conf/icip/icip2010.html#NelsonK10>.

Nico, G., Tome, R., Catalao, J., Miranda, P., 2011. On the use of the WRF model to mitigate tropospheric phase delay effects inSAR interferograms. IEEE Trans. Geosci. Remote Sens. 49, 4970–4976. http://dx.doi.org/10.1109/TGRS.2011.2157511.

Perissin, D., Rocca, F., Pierdicca, M., Pichelli, E., Cimini, D., Venuti, G., Rommen, B., 2011. Mitigation of atmospheric delay in InSAR: the ESA Metawave project. In: Geoscience and Remote Sensing Symposium (IGARSS), 2011 IEEE International, pp. 2558–2561. http://dx.doi.org/10.1109/IGARSS.2011.6049734.

Pierdicca, N., Rocca, F., Basili, P., Bonafoni, S., Carlesimo, G., Cimini, D., Ciotti, P., Ferretti, R., Marzano, F., Mattioli, V., Montopoli, M., Notarpietro, R., Perissin, D., Pichelli, E., Rommen, B., Venuti, G., 2011. Synergic use of EO, NWP and ground based measurements for the mitigation of vapour artefacts in SAR interferometry. In: Geoscience and Remote Sensing Symposium (IGARSS), 2011 IEEE International, pp. 2566–2569. http://dx.doi.org/10.1109/IGARSS.2011.604976.

Rüeger, J.M., 2002. Refractive index formulae for radio waves.

Selesnick, I., Baraniuk, R., Kingsbury, N., 2005. The dual-tree complex wavelet transform. IEEE Signal Process. Mag. 22, 123–151. http://dx.doi.org/10.1109/MSP.2005.1550194.

Selesnick, I.W., 2002. The design of approximate Hilbert transform pairs of wavelet bases. IEEE Trans. Signal Process. 50, 1144–1152 (see also IEEE Transactions on Acoustics, Speech, and Signal Processing) <http://ieeexplore.ieee.org/xpls/abs_all.jsp?arnumber=995070>.

Smith, E., Weintraub, S. (Eds.), 1953. The Constants in the Equation for Atmospheric Refractive Index at Radio Frequencies.

Ulmer, F.G., Adam, N., 2015. A synergy method to improve ensemble weather predictions and differential {SAR} interferograms. {ISPRS} J. Photogramm. Remote Sens. 109, 98–107. http://dx.doi.org/10.1016/j.isprsjprs.2015.09.004 <http://www.sciencedirect.com/science/article/pii/S0924271615002051>.